Journal of Sailing Technology 2025, volume 10, issue 1, pp. 143-170.
The Society of Naval Architects and Marine Engineers.

Hydrofoils Design and Multifidelity Optimization for a Flax Fiber Moth

Michele Bonetti
Audace Sailing Team, University of Trieste, Italy, michele.bonetti@outlook.it

Barnaba De Carli
Audace Sailing Team, University of Trieste, Italy.

Andrea Parmegiani Della Corte
Audace Sailing Team, University of Trieste, Italy.

Mitja Morgut
University of Trieste, Italy.

Enrico Nobile
University of Trieste, Italy.

Manuscript received April 27, 2025; revision received June 12, 2025; accepted July 5, 2025.

Abstract.

Can sustainability enter the world of high-performance sailing? This paper explores the use of flax fiber composite as a feasible alternative to traditional materials in the design of sailboat components, focusing on an International Moth prototype. A hydrofoil design process was developed, integrating flax fiber composite in proportions exceeding 50% by weight—an approach that represents one of the first attempts of its kind. A multifidelity strategy was adopted and embedded within a concurrent engineering workflow tailored to the project. Starting with accessible design tools such as XFOIL and XFLR5, both two and three dimensional analyses were conducted to define the initial configuration. A Static Velocity Prediction Program was also implemented to evaluate hydrofoil performance in realistic conditions, accounting for finite wing effects, hull drag, and sail thrust. The preliminary design was further refined using a design exploration software (modeFRONTIER), enabling the evaluation of thousands of combinations of key geometric parameters through a multi-objective optimization process which included structural constraints. A high-fidelity optimization phase followed, using CFD simulations on parametric foil models, focusing only on the most promising parameter ranges to reduce computational cost. The resulting workflow proved effective in delivering a set of hydrofoils that demonstrate the feasibility of sustainable composites for competitive, high-performance sailing applications.

Keywords: hydrofoil, parametric design, multifidelity optimization, CFD, flax fiber composite, moth

NOMENCLATURE

A	Area [cm^2]
b	Wing span [mm]
c - c_{root}	Section - Root section chord [mm]
C_D	Drag coefficient [-]
C_{Di}	3D drag coefficient correction for induced drag [-]
C_L	Lift coefficient [-]
$C_{L,0^\circ}$	Zero angle of attack lift coefficient [-]

$C_{L,3D}$	3D corrected lift coefficient [-]
d	Anhedral depth [mm]
L/D	Lift over drag ratio or hydrodynamic efficiency [-]
N_{crit}	Variable used in XFOIL to quantify free flow turbulence [-]
Re	Reynolds Number
t/c	Thickness to chord ratio [-]
α	Angle of attack [°]
α_{flap}	Flap deflection angle [°]
Δ	Delta, wing planform shape parameter [-]
λ	Wing geometric aspect ratio [-]
ρ	Fluid density [kg m^{-3}]
2D	Two-dimensional
3D	Three-dimensional
AST	Audace Sailing Team
CAD	Computer-Aided Design
CAE	Computer-Aided Engineering
CFD	Computational Fluid Dynamics
CFRP	Carbon Fiber Reinforced Plastic
DVPP	Dynamic Velocity Prediction Program
FEM	Finite Element Method
IMCA	International Moth Class Association
LE	Leading edge
NACA	National Advisory Committee for Aeronautics
MF	Main Foil
MOGA	Multi Objective Genetic Algorithm
ORC	Offshore Racing Congress
RANS	Reynolds Averaged Navier Stokes equations
RF	Rudder Foil
RSM	Response surface model
SMC	Sustainable Moth Challenge
TBS	True Boat Speed
TE	Trailing edge
TWS	True Wind Speed
VPP	Velocity Prediction Program

1 INTRODUCTION

A Moth is a single-handed monohull which, thanks to its small size and the design freedom ensured by its development class status, has become since the 2000s a testing ground for hydrofoil innovations. Notably, the most important stages of high-performance sailing scene – such as SailGP and America's Cup – are now dominated by former Moth sailors. Even the research community is not immune to the charms of this little foiler (Binns et al., 2008; Findlay and Turnock, 2008; Beaver and Zseleczky, 2009; Eggert, 2018; Day et al., 2019; Bagué et al., 2021; Guedes Soares and Santos, 2022).

Today's Moths are incredibly fast and lightweight: they are entirely made of carbon fiber and highly engineered, reaching prices up to fifty-thousand euros in the high-end range. This recent trend is leading to a restriction of the audience who can compete at a high level in this class, pushing the development of more affordable alternatives – such as the Waszp and, more recently, the Switch – with a *one-design* philosophy. Moreover, these small boats have a significant environmental impact.

In 2019, the idea of proposing a design challenge emerged: to create high-performance Moths with

alternative technologies and solutions that include sustainability into the design process. SuMoth Challenge (SMC) was founded with this goal by Bruno Giuntoli, an Aerospace engineer previously involved in a C-Class Catamaran Project. This student-oriented competition is set within the context of the Foiling Week, arguably the biggest event entirely dedicated to hydrofoils designers, manufacturers, and sailors, which takes place every summer in Italy. The SMC reflects a growing awareness on the environmental impact of the sailing industry (11th Hour, 2022; Website, 2024). Energy intensive materials such as carbon fiber, disposable plugs and moulds, and the widespread issue of recycling fiber-reinforced composites are just some examples of the environmental impact associated with racing and recreational sailboats. However, almost 15 years have passed since the first experiment of natural fiber composites on sailboats (Pourcheron, 2010): since then, applications have been limited to small prototypes (Castegnaro and Basile, 2017; AST, 2025), with some valuable exceptions (NLcomp, n.d.; Greenboats, 2025).

Within this context, Audace Sailing Team (AST) from the University of Trieste accepted the challenge, choosing flax fiber composite to design and build its own International Moth concept (Fig. 1). A detailed overview of the entire design and manufacturing process can be found in Bonetti (2024). Hereafter, the focus is on fully submerged hydrofoil design: the idea is to describe a complete workflow, starting from inspirations and first sketches all the way down to the final optimized models. On hydrofoils applications for sailing boats, available literature is quite extensive (Beaver and Zseleczky, 2009; Findlay and Turnock, 2008; Day et al., 2019; Tannenberg et al., 2023): however, it seems to lack of a comprehensive description of hydrofoil design process, which is exactly the aim of this paper. In order to achieve this goal, a *designer approach* is adopted: after an in-depth overview of the state of the art, key issues are identified and translated, first as design goals and then into measurable properties of the hydrofoils, creating a multidimensional design space to be explored.

A *multifidelity* framework is described, starting with simple and effective tools and slowly adding complexity while converging toward the final configuration. An attempt is made to overcome the traditional *design spiral* (Larsson et al., 2022), relying on a systematic design space exploration inspired by *decision-based design* (Trincas, 2022) and boosted by optimization strategies. This approach has been key to develop, in a very short time, a sufficiently clear idea of how to design hydrofoils for a sailing boat, something we knew very little about before.

Figure 1. AST Sustainable Moth, *Bai-Flying Lina* (Garda Lake, 2023).

Also, compensation for the use of less performing fibers on hull and hydrofoils is addressed by incorporating specific constraints and parameters, allowing to manage this additional challenge and differentiate the design from existing carbon boats. Among the available alternatives, flax fiber composites have attracted increasing attention in the marine sector as a potentially more sustainable option. However, their use comes with notable challenges. Studies by Baley et al. (2019), Baley et al. (2020), and Davies et al. (2022) point out the variability in mechanical properties due to factors such as fiber treatment, extraction method, and environmental conditions—issues that directly affect structural reliability. Similarly,Blier et al. (2025) provide an application-oriented assessment of flax composites in boatbuilding, emphasizing the need for case-specific testing rather than general assumptions about performance. In parallel, Souppez et al. (2025) address the regulatory limitations currently affecting the adoption of these materials, suggesting that broader integration into design standards will be necessary before widespread use is feasible. Overall, while flax composites cannot yet replace carbon fiber in all respects, their inclusion in a student-led design project offers an opportunity to engage with material limitations while exploring realistic paths toward lower-impact solutions.

The overall result is an effective workflow that was easily integrated in the overall Moth design and manufacturing campaign, adopting *concurrent engineering* to progress simultaneously with design and production of the different parts. Just 8 months after the beginning of the project, AST joined the SuMoth Challenge, with a functioning prototype.

The rest of the paper is organized as follows. In §2, after a preliminary overview, goals and constraints are identified and the starting design space is set. Hydrofoils key features are explored in §3. Different foil sections are collected in a database and compared using *XFOIL*, to select a suitable two-dimensional (2D) shape. Then, a first comparative analysis on hydrofoil performance in real conditions is made using a basic Velocity Prediction Program (VPP), built in-house as an Excel workbook. The program is based on simple equations which include 2D numerical data, finite wing corrections, hull drag and sail thrust. This preliminary analysis leads to assess an acceptable range for the main dimensions. three-dimensional (3D) shapes are then sketched and compared in *XFLR5*, resulting in a baseline model to be used as a starting point for the optimization process. Two parametric models are created using *Grasshopper* (§4), to be tested with an *isolated wing* Computational Fluid Dynamics (CFD) template. This model is tailored to deliver acceptable results in less than one hour runs, on a student laptop. Before starting with high fidelity optimization, §5.1 features a low fidelity stage: the whole design space is explored, implementing the VPP described above in *modeFRONTIER*. This design exploration software allows to perform an automated design of experiment with over 1000 samples, to identify the most promising ranges of each parameter. Then, a more complex design process is created (§5.2): each foil is tested in two typical operating conditions (take-off and downwind foiling), using a commercial CFD solver (*Simcenter Star-CCM+*). Variables studied in the two-objective optimization are not only Grasshopper geometric parameters but also working angles, including optimal flap deflection range. After a CFD validation of the results, planform shapes are defined for both rudderfoil and mainfoil (§6), and complete geometries, including bulbs, are refined in *Rhinoceros*. Other important aspects are mentioned, such as rudder and centreboard design, and the relative placement of both rudderfoil and mainfoil, with respect to the hull and the sail plan: vertical and longitudinal position, struts length and forward rake are defined in this stage, to ensure a well balanced boat and steady foiling. Finally, structural design and production are briefly described. Conclusions and future developments are summarized in §7.

2 DESIGN STRATEGY

The overall goal of the project was to design and build an International Moth prototype. The first and most radical decision was to choose flax fiber – coupled with bio-based epoxy resin – as the main building material, both for the hull platform and for the foils. This idea came from previous experiences in the field of natural composite materials, having built two 15 feet skiffs with flax fiber for the 1001VelaCup competition. Following this choice, the Team had to work his way to craft a

reasonably fast, easy to handle boat, designed to be built with reduced costs and a restricted access to high-tech facilities, resulting in a KISS approach (*Keep it simple, stupid!*, a motto learned during the SMC Masterclass program, SuMoth Association (2022)).

2.1 State of the Art Overview

An overview of the existing International Moth fleet and manufacturers was carried out, focusing on the most successful Moth concepts: from classic Mach2 to latest boats, such as Bieker, Aerocet, Manta, and Swift. Full scale measurements were made on boats available to the team as a benchmark. As shown in Figure 2, an obvious trend was noticed in foil design, evolved toward smaller foils with thin sections and relatively high span. Typical tandem foil architecture, with fully submerged T-foils, is the only configuration available on the market. The same configuration is adopted in our project, saving for possible future developments more “aggressive” concepts like *ladder* foils (Speer, 2001), *morphing* foils (Gon, 2021; Muzio, 2021; Giovannetti, 2017) or *split flaps* (Prabahar et al., 2022).

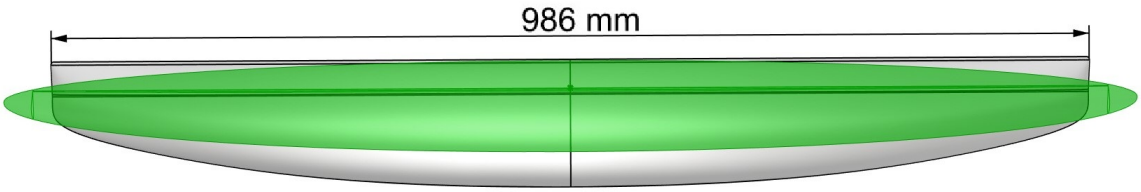

Figure 2. 2009 Hungry Beaver (grey, 1030 cm^2) vs 2022 commercial mainfoil (green, 800 cm^2).

2.2 Constraints: Class Rules, Budget and Time

To correctly set the boundaries of the design space, external and internal constraints were identified as soon as possible. As a matter of fact, a *SuMoth* prototype has to comply not only with the *Class Rules* from the International Moth Class Association (IMCA), but also with specific rules set by the SMC organization itself (IMCA, 2017; SuMoth Association, 2024). Moreover, the “sustainability budget” was especially challenging: each team is assigned 10,000 SuMoth Dollars (SM$), a fictional currency used to compute the economic and environmental impact of the project. In addition to that, explicit limits are imposed to the use of carbon fiber, for key components like hull and foils (see Tab. 1). Low budget and limited access to advanced manufacturing methods are also a common issue for student projects: in this framework, the sustainable approach encouraged by the competition, which included reusing and recycling, can help cutting costs. Finally, the entire project, from the first draft to the final product, had to be completed in only eight months: shortage of time was a push to experiment an integrated approach, overlapping design and production phases within the same *Gantt diagram*.

Table 1. Carbon fiber reinforced plastic limitations, % by weight (SuMoth Association, 2024).

CFRP	Hull	Hull wings	Centreboard	Mainfoil	Rudder	Rudderfoil	Rig	Other
Virgin	5%	5%	50%	50%	50%	50%	100%	50%
Recycled	10%	20%	60%	60%	60%	60%	100%	60%
Upcycled	100%	100%	100%	100%	100%	100%	100%	100%

2.3 Designing with Flax Fiber: Challenges and Rewards

The imposed limit to the use of carbon fiber demands to move beyond the industry standard of pre-impregnated high modulus fibers, adopting a new approach to material choice. For this project, a blend of carbon and flax fiber was chosen: the goal was to have a finished product which contains more than 50% by weight of flax fiber composite. To the best of the authors’ knowledge, the one here presented is the first attempt to include natural fiber composites in hydrofoil design.

Table 2. Starting design space.

2D geometry (airfoil)	Min	Max	Step
Thickness over chord (t/c, %)	6%	15%	2%
Thickness position (% c)	30%	60%	10%
Camber ($C_{L,0^\circ} \times 10$)	0	6	1
Max camber position (% c)	15%	50%	*Variable*
Flap length (% c)	10%	40%	5%
Angle of attack (α, $^\circ$)	- 10°	10°	0.5°
Flap Angle (α_{flap}, $^\circ$)	- 10°	15°	0.5°
3D geometry (planform)	Min	Max	Step
Span (b, mm)	900	1150	50
Area (A, cm^2)	850	1050	50
Flap length (% c_{root})	25%	45%	5%
Shape parameter (Δ, % c_{root})*	25%	75%	5%
Flow properties (freshwater)	Min	Max	Step
Speed (kn)	3	30	*Variable*
Reynolds number (Re)	1.5×10^5	1.5×10^6	*Variable*
Flow transition ($N_{\text{crit}} = 1 \div 9$)**	4	4	-

*Δ is a non-dimensional parameter which defines the foil planform shape (see §4 for details).

**N_{crit} is used in XFOIL and XFLR5 to assess laminar to turbulent transition (see §3.1 for details).

Moreover, as mentioned before, flax fiber was selected as the main ingredient also for hull construction, including deck, hull wings and internal structures. This material choice had a big impact on the whole project. The effect went far beyond the obvious concerns on structural reliability, affecting also the hydrodynamic design and optimization. For instance, a heavier than average boat calls for bigger lifting surfaces, while the lower stiffness of the foil structure can lead to discard excessively thin sections and high aspect ratios.

2.4 Goal Setting

Being aware that it is difficult, for a flax fiber boat, to be as fast as a full-carbon one, the focus was shifted to light wind performances and ease of use, rather than pursuing high speeds at all costs. The main goals, determined at the end of this preliminary stage, are summarized below:

1. *Lightweight, in a sustainable way*: A 50 kg boat, rigged and ready to sail, is the final target;
2. *Structural reliability*: Together with proper hull structural design, a thickness constraint was established on both foils and struts sections and bending stiffness was taken into account during the geometry optimization;
3. *Ease of building and Cost reduction*: The applied *design for construction* approach means choosing solutions which can be implemented through simple processes and proven techniques, promoting upcycling and reuse of scrap material too: almost all manufacturing processes for the Moth have been in-house and took place at the Eco Sailing Lab, located in the university campus.
4. *Early take-off and Easy foiling*: To ensure suitability for unexperienced foiling sailors, extra stability and ergonomics were sought, resulting in increased hull beam and low tilt angle wings. The need for easy use was balanced by the desire to have a boat capable of getting up on the

foils even in lighter breeze. Higher span foils, with relatively big areas, were the chosen path to reach both goals, together with a low drag optimized hull shape.

2.5 Hydrofoils Design Roadmap

Having these goals and constraints in mind, an initial design space was created, translating qualitative statements into a set of parameters (Tab. 2). Hydrofoil design process was divided into three stages: a *baseline design* phase, to gather information and define a starting concept; an *advanced design* phase, featuring both low fidelity and high fidelity optimizations; a *detailed design* phase, including shape refinements, foils position and resulting interaction with hull and sail. Production issues were also addressed in this stage, before the manufacturing phase could finally start.

3 BASELINE DESIGN

This conceptual phase aimed to provide the necessary information to set a reliable baseline geometry for both mainfoil and rudderfoil, from which to start parametrization and optimization processes. In-depth investigation on preliminary analyses can be found in Parmegiani Della Corte (2023).

3.1 2D Airfoil Selection with XFOIL

The starting point to design a wing is usually the definition of the section profile. Only existing profiles were selected and tested: the creation of new airfoils was left as a future upgrade. Two-dimensional analyses were carried out using XFOIL: this is an open source software from MIT, which delivers a benchmark for airfoils at low angles and Reynolds number (Re) between 10^5 and 10^6. The computational structure is based upon the *ISES code*, an algorithm developed at MIT by Drela (1989) and Yiu and Giles (1995), suitable to predict flow around an airfoil at very low Reynolds numbers ($< 5 \times 10^5$). This code uses a viscous-inviscid zonal approach: outside the boundary layer the two-dimensional flow is inviscid, and thus described by *potential flow* theory; inside the boundary layer, the viscosity is considered using two equations, one for the momentum and one for the kinetic energy. Internal (viscous) and external (inviscid) flow are fully coupled in the solution scheme. The transition point between laminar and turbulent flow can be imposed at a specific location or predicted using an amplification formulation based on small disturbance theory (e^n criterion, with $n = N_{\text{crit}}$ as tuning variable).

Airfoils were collected both from available literature (as the free website *Airfoil Tools*), as well as full scale measurements from existing hydrofoils. The database was set within the ranges specified in Tab. 2 and included 35 different sections, divided into two groups: symmetric for rudder and centreboard, asymmetric for mainfoil and rudderfoil. Hereafter, only asymmetric airfoil selection for the hydrofoils is described; symmetric sections were studied following the same logic, and results are shown in §6.3.1.

For this application, there isn't only one design condition to be studied, in terms of angle of attack (α) and flap deflection (α_{flap}). In fact, a Moth does not have a specific cruise speed but, once up on the foils, it can sail from 10 kn to more than 25 kn of true boat speed (TBS), depending on wind intensity and course. Lift force has to be kept to a constant value, and this is achieved in three ways: the mainfoil features an integrated flap, which automatically reduces lift as a function of ride height, doing a great part of the job; additionally, rudder rake, and thus rudderfoil α, can be manually modified by the helmsman; finally, shifting weight – moving the body forwards or backwards – results in a trim variation which changes the angle of attack for both foils (Neri, 2024).

Lacking of previous experience of foil design, suitable ranges of α and α_{flap} were not set in advance; instead, these variables were explored within a wide range (Tab. 2), using available benchmarks as a guideline (Beaver and Zseleczky, 2009; Day et al., 2019). Target lift coefficients, which depend on foil size, were estimated using an in-house tool, later described in §3.2. To compute a two-dimensional lift coefficient (C_L) for XFOIL, the following assumptions are adopted here: a 130 kg design weight (fully

rigged boat with sailor onboard), with about 80% of the lift provided by the mainfoil ($L_{\text{mf}} \approx 1000$ N), a reference mainfoil area of 950 cm^2 and some lift force loss (15 to 20 %) due to finite span effects.

The study covers Reynolds numbers (Re) up to 1.5×10^6, but the main focus is on the lower speed range, in accordance with design goals set in §2. Considering a reference airfoil chord of 8 cm – which is a plausible value for the mainfoil mean chord – a TBS of 8.5 kn corresponds to $Re \approx 3.5 \times 10^5$, matching take-off conditions. Tuning parameter for laminar to turbulent transition is set to $N_{\text{crit}} = 4$, to mimic foiling in open water environment (Drela and Youngren, 2001).

3.1.1 Comparison: NACA vs Eppler

To understand the correlation between geometry and performance, a systematic analysis was carried out on the *6-series* of the NACA (National Advisory Committee for Aeronautics) database, by varying: position of maximum thickness (related to the second digit), camber (related to the third digit) and thickness over chord ratio (expressed in % by the last two digits). Three groups, showing the most interesting performances, were selected from the broader matrix for further investigation: one from the 63 family (NACA 63412-63612), and two from the 64 family (NACA 64306-64310-64312, NACA 64610-64612-64615). After imposing a limit on thickness over chord ratio ($t/c \geq 11\%$), as a safety measure to account for the use of flax in place of carbon fiber, the best NACA airfoils were found to be NACA 64612 and NACA 63412. Regarding the Eppler group, the choice fell on Eppler 393. Its airfoil shape is reported in Figure 3, in comparison with that of NACA 63412.

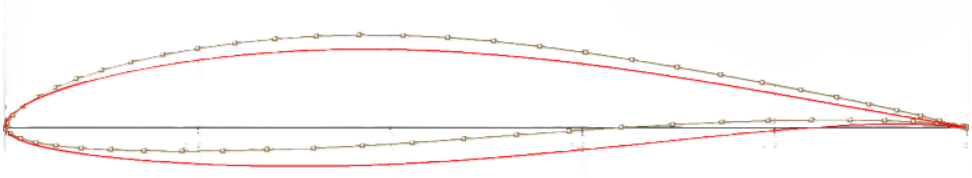

Figure 3. Eppler 393 (red) and NACA 63412 (brown) geometries (XFLR5).

Figure 4 displays performance comparison for Eppler 393, NACA 64612, NACA 63412, and other benchmark airfoils, at $Re = 4.5 \times 10^5$. Studying undeformed airfoils (i.e. without flap) at this Re – resulting to roughly 11 kn speed for a 8 cm chord – is consistent with the goal of seeking good performances in marginal foiling conditions, since the highest mainfoil efficiency is normally achieved with little flap deflection. This comparison is also useful for the rudderfoil, which doesn't feature a flap. With equal α (Fig. 4, left), Eppler 393 shows the highest efficiency (L/D) over the expected operating ranges, for both mainfoil ($0° < \alpha < +5°$) and rudderfoil ($-5° < \alpha < +5°$). If a target lift coefficient is set ($C_L = 0.67$), only NACA 64612 has a slightly lower drag coefficient (C_D, see Fig. 4, right), yet with a notably higher angle of attack: this is likely to affect performances at higher speeds, due to the larger flap deflection needed.

To explore actual operating conditions for the mainfoil, across the entire range of speeds, the presence of an integrated flap was included in the study. Three different flap lengths were considered: 20%, 30% and 40% of the chord. Initial analysis was carried out in a wide range of α_{flap} (-10° to +15°) to replicate the entire range of movement of the flap in all possible conditions. Special attention was paid on combination of high α and α_{flap}, to avoid flow separation and stall. Eppler 393 showed again the highest L/D among the studied airfoils. Figure 5a shows computed curves for Eppler 393, with 30% flap length and α_{flap} from 0° to 10°. Reynolds number corresponds to take-off speed, which is a critical condition to ensure the *easy take-off* goal. With a target lift coefficient set to $C_L = 1.33$, the best take-off combination for Eppler 393 appears to be: $\alpha = 3°$ and $\alpha_{\text{flap}} = 8°$.

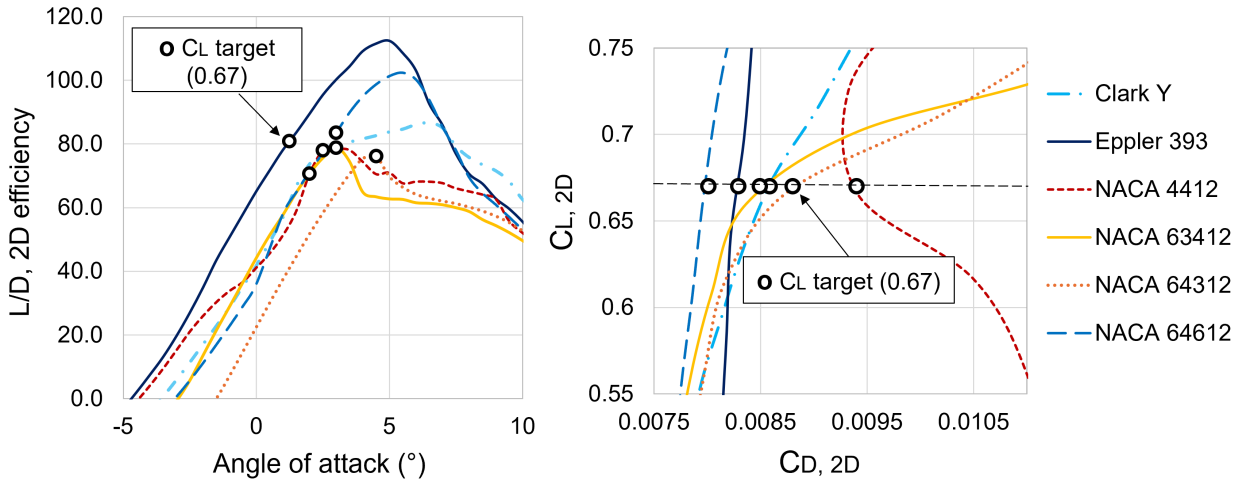

Figure 4. Airfoil comparison without flap, light wind conditions (XFOIL: $Re = 4.5 \times 10^5$, $N_{\text{crit}} = 4$).

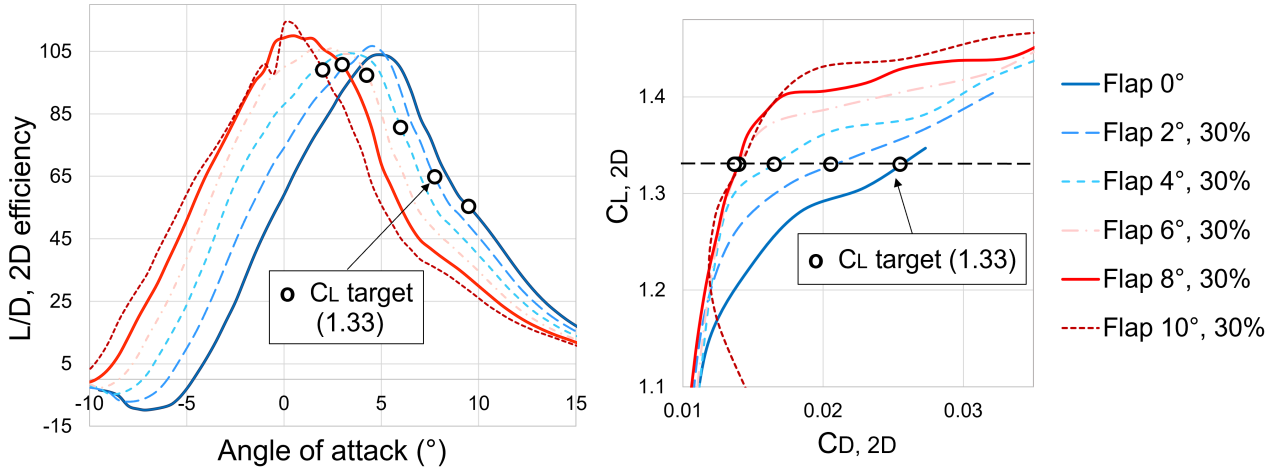

(a) Eppler 393, flap length 30%, flap deflection from 0° to 8°.

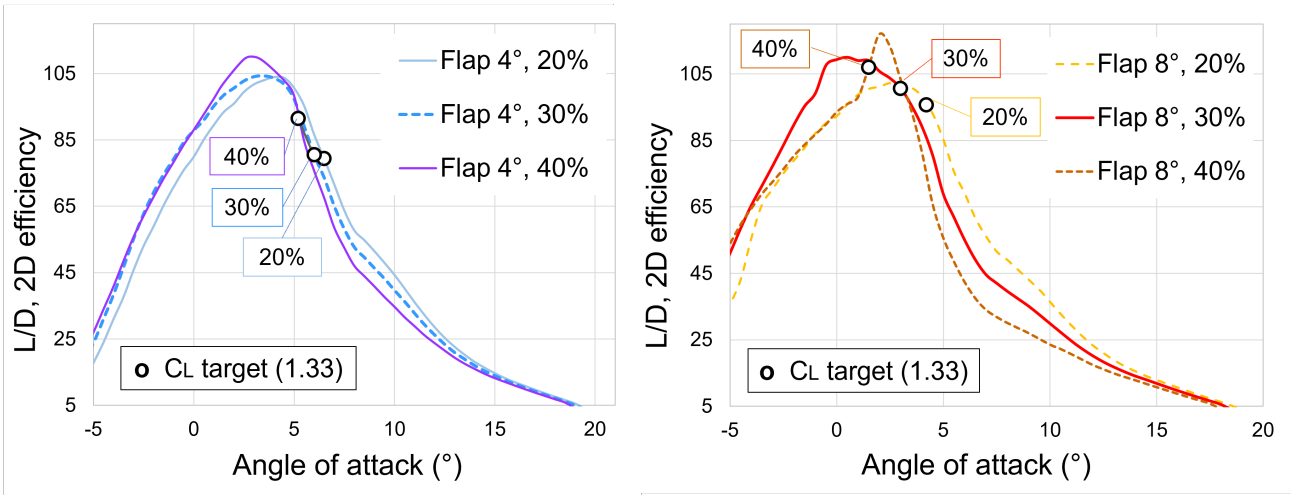

(b) Eppler 393, flap length from 20% to 40%, flap deflection 4° and 8°.

Figure 5. Eppler 393 with integrated flap, take-off conditions (XFOIL: $Re = 3.5 \times 10^5$, $N_{\text{crit}} = 4$).

A 40% flap seems to further improve efficiency in these conditions (see Fig. 5b), although the curve for $\alpha_{\text{flap}} = 8°$ shows some unevenness, suggesting that the reliability of a tool like XFOIL can be affected by working in the upper range of α_{flap}. Therefore, flap length is kept as a variable to be further investigated (see Tab. 3 in §5.1).

As a result of the study described in this chapter, Eppler 393 was chosen to build the wing section for both mainfoil (with an integrated flap) and rudderfoil (without flap). The profile shows high efficiency at lower speeds- higher C_L values (i.e. heavily loaded wing). Furthermore, it seems to perform well also across the entire range of angles and Re studied: this robustness is important because target α and α_{flap} for each speed will be precisely identified only at the end of the optimization process.

3.2 VPP-driven Assessment of Foils Size

A simple performance prediction program – basically, an Excel workbook – was created using elementary aerodynamic equations, integrated with Eppler 393 airfoil data from XFOIL and experimental correction coefficients from literature (Beaver and Zseleczky, 2009). Input parameters defined for the analysis included: mainfoil planform area (A) and span (b), rudderfoil A and b; lift ratio, as the percentage of the total load carried by the mainfoil; maximum values for mainfoil and rudderfoil α and for mainfoil α_{flap}, all expected during the take-off phase (boat trimmed by the stern). From zero up to 25 knots, the desired outputs were calculated: overall lift and drag of foils and struts, accounting for 3D effects; target mainfoil α in foiling mode; α_{flap} and rudderfoil α required for each foiling speed, resulting from constant lift constraint. Figure 6 shows an example of lift and drag curves computed for a tested pair of mainfoil and rudderfoil. The shaded area indicates the expected take off threshold: at lower speeds each angle is fixed to its maximum value, which has been defined as input; instead, after take off the equilibrium condition is found by computing α_{flap} (for the mainfoil) and α (for the rudderfoil), to match the required lift coefficient for both foils at each speed. The sudden drop in vertical struts drag after take off is due to draft change, and the resulting reduction of wetted area. Only upright conditions (i.e. zero heel) are considered within this model.

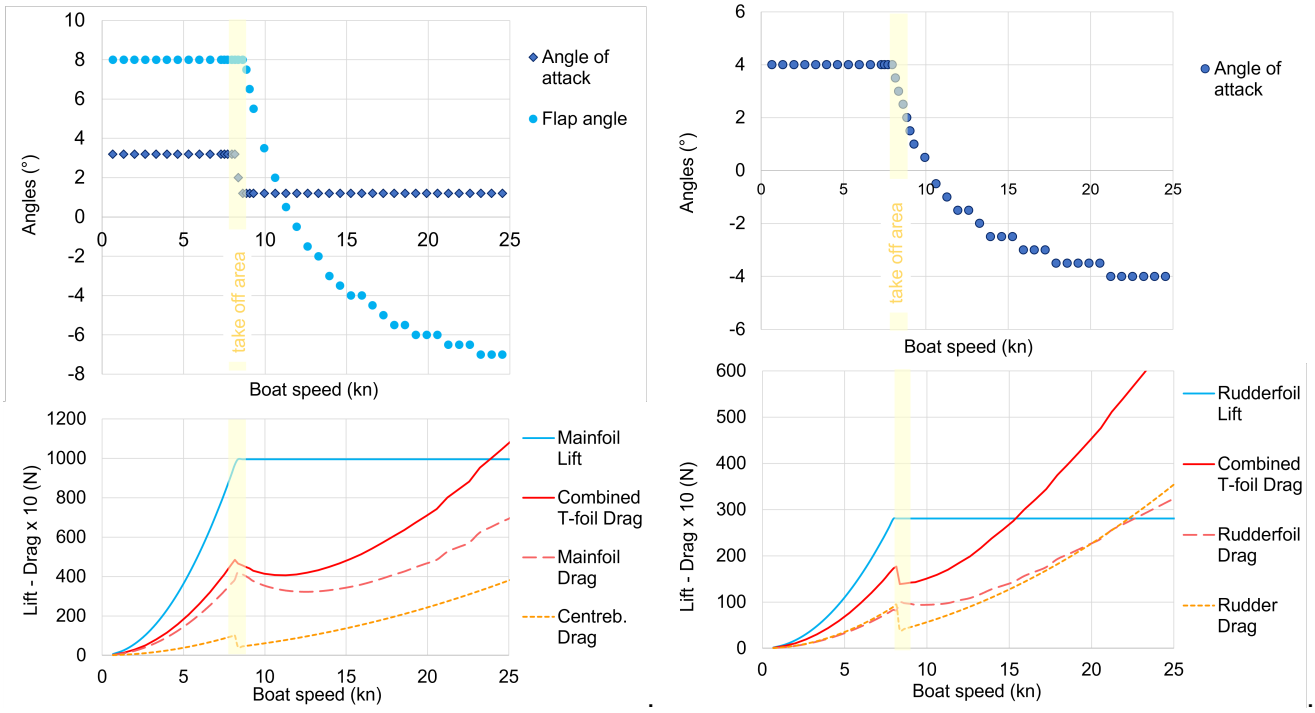

(a) Mainfoil **(b)** Rudderfoil

Figure 6. Example of foils performance prediction (data from in-house VPP).

To obtain 3D corrections for lift and induced drag coefficients, the following equations were used (Nobile, 1954), assuming elliptical lift distribution and introducing geometric aspect ratio as $\lambda = b^2/A$:

$$\begin{cases} C_{L,3D}(\alpha) = \dfrac{C_{L,2D}(\alpha)}{1 + \dfrac{2\,(1 + 0.77\,t/c)}{\lambda}}\,, \\ \\ C_{Di}(\alpha) = \dfrac{C_{L,3D}^2(\alpha)}{\pi\lambda}\,. \end{cases} \tag{1}$$

The model includes an estimation of hull resistance at different speeds and variable displacements, with experimental data from Beaver and Zseleczky (2009). The aim is to correctly capture the total drag progression – which is the real variable to be minimized – describing its variation from displacement (hull + appendages) to foiling mode (only appendages), with the typical drag "hump" (Figure 7).

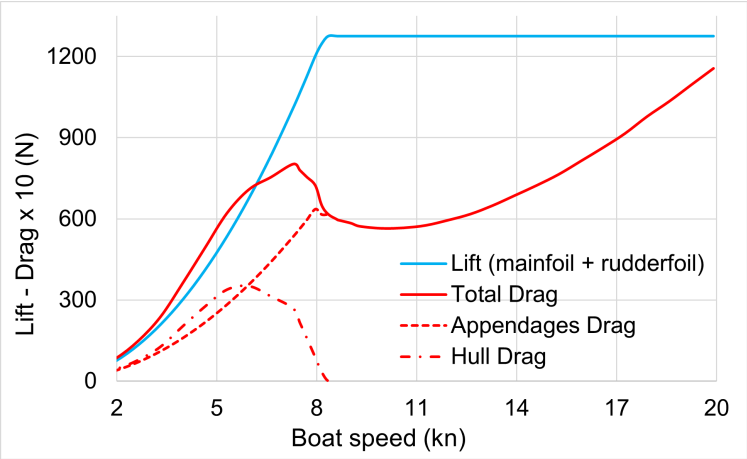

Figure 7. Lift and drag composition, (data from in-house VPP).

An estimation of sail thrust is also computed, using literature coefficients from Offshore Racing Congress VPP (ORC, 2016): the coefficients used are the ones for the *high lift mainsail*. Sail thrust is obviously related to wind speed, and it balances the overall resistance of hull and appendages: in particular, to ensure take-off, the maximum thrust available has to be greater than drag value at the "hump". In this way, marginal foiling conditions may be predicted, as showcased in the results (Fig. 19).

Finally, a structural design worksheet was added to account for material properties. The foil is modeled as a variable section beam, with a heterogeneous section made by a shell of carbon fiber reinforced plastic (CFRP) and a core of flax fiber composite. Through simple beam calculations maximum deflection is computed for both foils and a constraint is set, limiting unfeasible values for span and area.

This in-house tool proved to be really useful in order to understand the actual behavior of a Moth at different speeds, identifying suitable ranges of α and α_{flap}. At this stage, the main goal was to get an initial assessment of foils size. Later, the tool was used again in the optimization process described in §5.1, to quickly explore the design space and perform a preliminary optimization on foils main parameters.

3.3 3D Shape Drafting with XFLR5

After gaining an understanding of acceptable ranges of foil area and span, the process went on with the exploration of other tridimensional features: chord distribution along the span, leading edge and trailing edge curvature, flap area etc. The brainstorming phase relied upon massive internet research as well as on-site visits to Moth sailors and foilmakers, e.g. Persico facilities and Garda Carbon Lab by Ferrighi brothers, designers of Manta Moth and Switch foiler.

During this concept stage, tests and drawing were performed within XFLR5, a very useful tool which integrates XFOIL capabilities with a 3D module and a few different *finite wing* numerical models (such as Lifting Line Theory and Vortex Lattice Method). These additional feature allows to picture a more realistic idea of hydrofoil efficiency, by including lift distribution along the span and its effects on drag, namely the *induced drag*, which is neglected in a 2D study. To ensure easy take-off in lighter winds, reducing induced drag becomes the main focus. In fact, at lower speeds, lift coefficient is higher, making this the dominant resistance component, while at higher speeds *friction* drag is more important.

These considerations led us to focus on bi-elliptical wing shapes (see §4.2) with high span values, both for mainfoil and rudderfoil. Archetypal example of this design are the WWII Spitfire planes, with their famous elliptic wing planform: one of the goals of this peculiar shape was, indeed, to minimize induced drag. The bi-elliptical shape was parametrized using an Excel sheet: this tool, based on simple equations, allows to quickly compute the xy coordinates needed to draw the wing planform in XFLR5, with different combinations of shape and span.

In Figure 8, an efficiency comparison on four test mainfoils is reported, with increasing wingspans ($b = 950 - 1150$ mm) and roughly the same planform areas ($A = 960 - 970\,\text{cm}^2$). Angle of attack is kept to a constant value of $\alpha = 1°$. Three different speeds, representing typical operating conditions are tested:

1. take off: TBS of 9 knots, maximum flap deflection ($\alpha_{\text{flap}} = +8°$, $C_L \approx 1.03$);
2. foiling in light air: TBS of 12 knots, no flap deflection ($\alpha_{\text{flap}} = 0°$, $C_L \approx 0.55$);
3. foiling in breeze: TBS of 18 knots, negative flap deflection ($\alpha_{\text{flap}} = -5°$, $C_L \approx 0.23$).

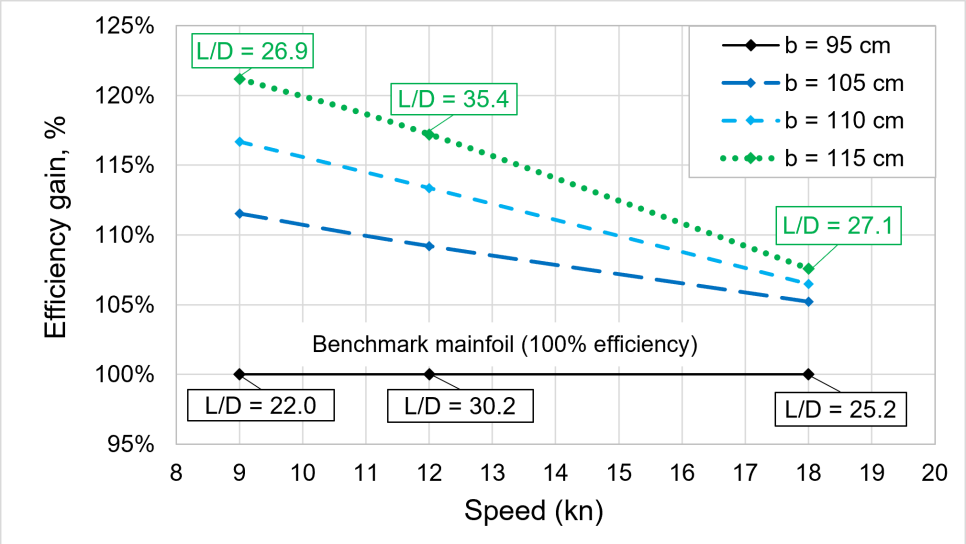

Figure 8. Mainfoil efficiency gain with increasing span (data from XFLR5).

Lift value is about the same in all tested conditions , representing a 130 kg displacement boat with about 80% of the lift provided by the mainfoil ($L_{\text{mf}} \approx 1000$ N). As expected, the best performance is achieved by the longest wingspan. Efficiency gain is particularly significant at lower speeds where, due to high C_L values, induced drag prevails: this is exactly the drag component which is reduced by increasing b, and thus λ (see C_{Di} formula in §3.2). The substantial impact of 3D effects on the overall resistance becomes evident by comparing these L/D values with the ones obtained from the XFOIL study (Figs. 4, 5). A baseline mainfoil, resulting from this first design stages, is showed in Fig. 9.

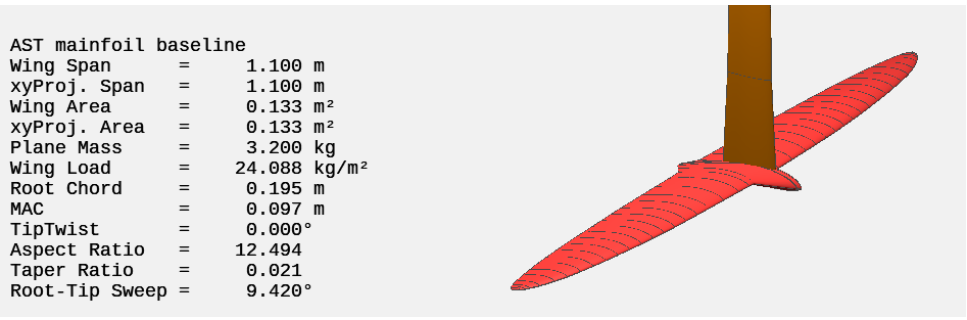

Figure 9. Mainfoil baseline design, wingspan = 110 cm (XFLR5).

4 FOILS PARAMETRIZATION

4.1 Parametric Design with Grasshopper

Grasshopper is a plugin for Rhinoceros, a popular CAD (Computer-Aided Design) software used in architecture, industrial design, and other fields that require the creation of complex models, including yacht design. This tool allows to create full parametric 3D models, that can be easily modified by using suitable parameters, directly linked to key geometric features. Grasshopper offers a visual programming interface within Rhinoceros. Instead of writing traditional code, users can create visual algorithms by connecting command blocks, known as *components*, to define relationships among 3D objects. For example, rather than writing lines of code to create a complex structure, designers can visually connect components that generate geometric shapes, control data flow, and apply transformations. This approach makes the creation of complex geometries and the automation of design processes within Rhinoceros more accessible. Moreover, the Grasshopper models can be complemented easily with Python scripts and linked with other CAE (Computer-Aided Engineering) tools. Parameters are adjusted through a slider, where a domain can be set: this is a very interesting feature, which fits well with the exploration and optimization logic used in our design process. In fact, Grasshopper itself can be easily integrated with optimization tools like modeFRONTIER.

Within AST projects, Grasshopper had been extensively used: both the skiff hull for 1001VelaCup and the Moth canoe body have been fully parametrized, with the aim of performing multi-objective optimization processes (Cantamessa, 2024). Taking advantage of previous experiences, hydrofoils geometries were studied in the same way.

4.2 Mainfoil and Rudderfoil Models

Two different Grasshopper files were created, one for the mainfoil and one for the rudderfoil. Resulting from the considerations described in §3.3, planform outline is composed by joining two semi-ellipses, one for the trailing edge (TE) and one for the leading edge (LE), forming a bi-elliptical shape. Thus, the parametrization itself becomes quite simple, because the ellipse equation gives a direct correlation between area and chord values.

For both mainfoil and rudderfoil, the surface is generated from two rail curves (LE and TE). A shape parameter called *delta* (Δ) defines these curves, by controlling the distance of the ellipse major axis from the TE: 0% means a straight trailing edge, while 100% means a straight leading edge. After defining the planform, a fixed number of Eppler 393 sections (21) is placed evenly across the span and then the surface is created using *Sweep2* command. Taking advantage of the symmetry, only half of the foils is actually modeled.

Mainfoil surface is controlled by the following parameters, as shown in Figs. 10 and 11: span (b), area (A), flap length (which indicates the hinge position in % of root chord), and delta (Δ), which, as explained above, controls the planform shape. Flap deflection parameter (α_{flap}) is also featured, in order to simulate different foiling conditions during the optimization process.

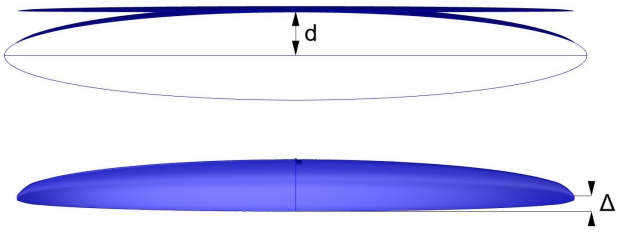

(a) *Rudderfoil, front and top view.*

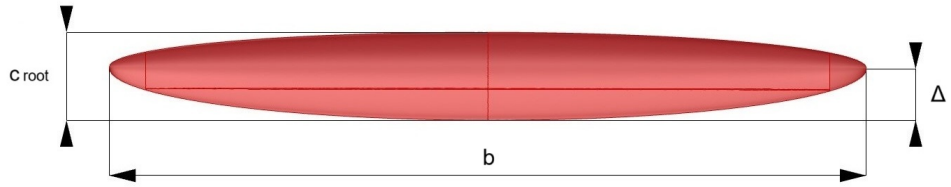

(b) *Mainfoil, top view.*

Figure 10. Hydrofoils parametric models (Rhinoceros).

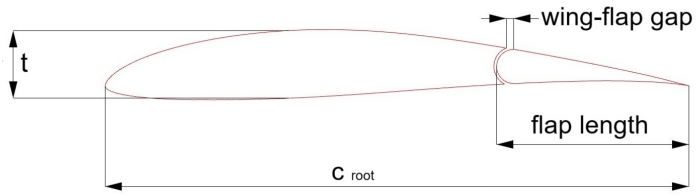

Figure 11. Mainfoil, root section with detached flap (Rhinoceros).

Flap surface is built in Grasshopper as an independent *closed polysurface*, detached from the rigid part of the wing. In this way flap deflection can be easily adjusted within the simulation routine (§5.2). To avoid interference problems, causing automated meshing within the CFD solver to fail, a small gap between the two parts is introduced, as visible in Fig. 11: however, its influence appears to be negligible for the purpose of the comparative analysis performed.

In an early design phase, another parameter was also investigated: winglets, to improve efficiency especially on the mainfoil. This possibility was later rejected in order to keep the building process as simple as possible, due to the quite small - at least in this case - drag reduction obtainable. An in-depth study on this topic can be found in Ferletti (2023).

Rudderfoil surface is defined using equivalent parameters, except for the ones related to the flap, which is not featured in this smaller hydrofoil. In addition to that, a second shape parameter is included in the rudderfoil modeling: anhedral depth (d). This additional variable represents leading edge curvature in the frontal plane (yz). Inspired by the so called *banana foils* shown in America's Cup concepts (Mozzy Sails, 2022), it was introduced for two main reasons: improving the bending stiffness of the rudderfoil, which is quite thin, by taking advantage of an arc shape; exploring possible advantages towards the occurrence of ventilation problems, keeping rudderfoil tips away from the water surface. In the Grasshopper workflow, this peculiar feature is parameterized using an ellipse, the anhedral depth (d) being its minor axis, as pictured again in Fig. 10a.

5 OPTIMIZATION SETUP

5.1 Low Fidelity Stage

A simple setup was created in modeFRONTIER, using the VPP described in §3.2: the aim was to explore and narrow down the design space in a quick and effective way. The optimization process was performed using MOGA-II (Multi Objective Genetic Algorithm), using as objective functions the appendages (foils + struts) drag in two different operating conditions: take-off phase and downwind drag. An additional constraint is imposed on target lift (1275 N), while varying the load ratio between mainfoil and rudderfoil. The algorithm generated and tested more than 1000 different combinations of the eight input parameters included in the VPP: mainfoil and rudderfoil span and area, maximum α_{flap}, maximum mainfoil and rudderfoil α, % of lift carried by the mainfoil (lift ratio).

Results are displayed in Fig. 12, where the obtained Pareto front (i.e. non dominated solutions) is highlighted. The outcome of this first optimization was needed to set a proper design space for the subsequent stage. Table 3 shows the input variables for the high-fidelity optimization: lift ratio is fixed, upper and lower bounds of the other variables are narrowed down, compared to the initial range of variation displayed in Tab. 2. Along with the eight inputs of the low-fidelity stage, four additional parameters (defined in §4) are included, as a result of the increased complexity of the model.

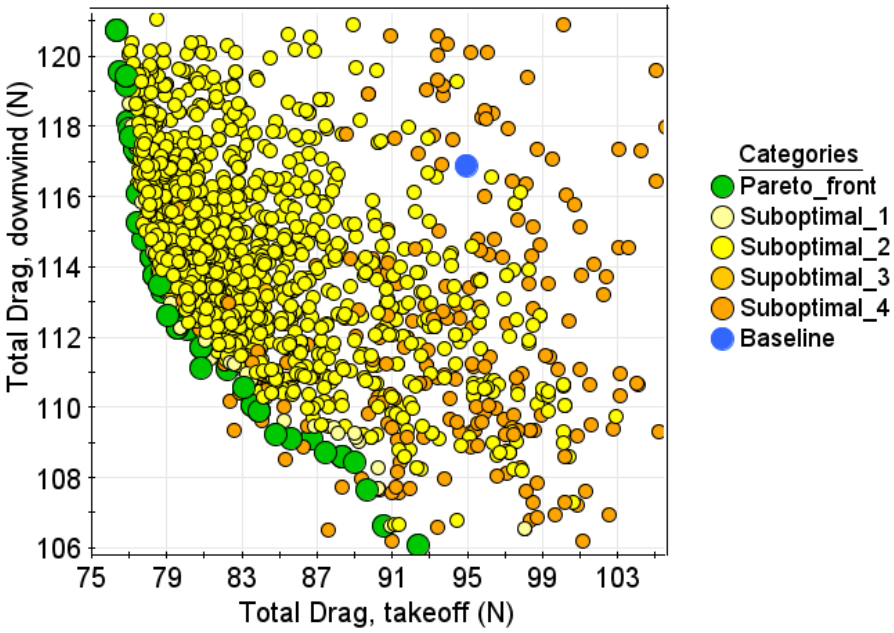

Figure 12. VPP driven design space exploration (modeFRONTIER).

5.2 High Fidelity Stage

5.2.1 Hydrodynamic Model in Simcenter Star-CCM+

The symmetry of the body and the absence of lateral (span-wise) component for the free stream velocity allows to assume a symmetric solution and hence to represent just half of the physical system. Additionally, since the main goal was to have a comparative analysis rather than an exact prediction of the performances as in other studies (Inguglia, 2021), the model includes the following assumptions:

- Each hydrofoil was studied as an isolated wing, neglecting both the interaction with the vertical strut and the downwash on the rudderfoil;

- As noticeable from Section 4, T-junction bulb was not included in the parametric model, reducing complexity and free variables; it was of course added later, in the final drawing.
- The free-surface effect on lift and drag was not explicitly taken into account, assuming it would have a similar impact on different designs.

As a result, each wing is modeled as a totally immersed body without free surface and without strut connection. In this way, despite representing only partially the real physics of the problem, we could obtain a consistent comparative study with a relatively low computational effort.

Table 3. Input parameters for the high-fidelity optimization.

	Baseline	Lower bound	Upper bound
Lift Ratio (% total lift)	78	-	-
A mainfoil (cm^2)	920	850	1000
b mainfoil (mm)	1100	1050	1150
max α mainfoil ($^\circ$)	4	3	5
max α_{flap}($^\circ$)	10	8	12
A rudderfoil (cm^2)	380	360	400
b rudderfoil(mm)	800	700	800
max α rudderfoil ($^\circ$)	4	3	5
Flap length (% c_{root})	35%	25%	45%
Δ mainfoil (% c_{root})	35%	25%	75%
Δ rudderfoil (% c_{root})	25%	25%	75%
d rudderfoil (mm)	60	50	80

The simulation focuses on the integral values of lift and drag. An additional control is set to check for potential cavitation condition. Cavitation is detected by monitoring the value of *total absolute pressure*: however, the occurrence of cavitation is unlikely within design conditions. The numerical setup involved the adoption of Menter's Shear Stress Transport turbulence model, or SST (Menter, 1994). The model combines the $k-\omega$ turbulence model and $k-\varepsilon$ turbulence model such that the $k-\omega$ is used in the inner region of the boundary layer, and $k-\varepsilon$ in the free shear flow. This model does not exhibits the strong free stream sensitivity of the $k-\omega$ turbulence model and improve the predictions of adverse pressure gradients. When compared to the $k-\varepsilon$ model, the SST model achieves better accuracy for attached boundary layers and flow separation. The thickness of the prism layer near the wall was set to obtain a value of y^+ below one, in order to better describe the boundary layer.

Both domain and mesh independence studies were performed, together with convergence evaluation (using turbulent kinetic energy as the target residual). However, since the goal was to analyze as many designs as possible within a fixed time, through an additional sensitivity study, the number of cells were reduced from 3.65 million to approximately 0.8 million cells (for the mainfoil model). Thus, a "lighter" mesh was employed, which was considered accurate enough for the comparative analysis performed. The final domain, box-shaped, has an overall size of 4.5 x 2 x 2.5 m (see Figure 13), with a *trimmed* type mesh. Stopping criteria were also set to further reduce computational effort: runs were stopped shortly after reaching convergence, counting 200 iterations in a range of variation of $\pm 1\%$ for the drag value. As a result, the time to run a full-scale simulation, on a typical engineering student laptop, varied between approximately 40-50 minutes for the mainfoil and 20-30 minutes for the rudderfoil (see Figure 14). The proposed CFD template has been validated using full scale experimental data, from Beaver and Zseleczky (2009). In-depth investigation on this topic is featured in De Carli (2024).

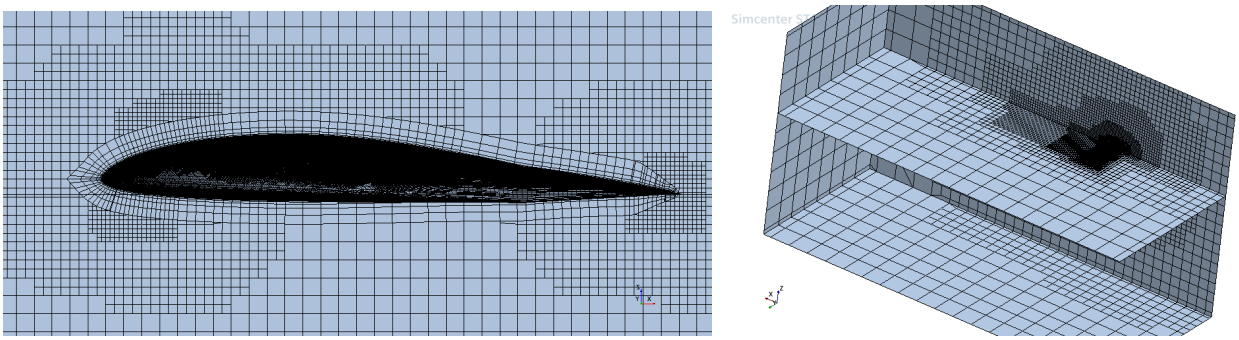

(a) *Mesh refinement and prism layer.* **(b)** *Global view of the domain.*

Figure 13. Trimmed mesh setup (Star-CCM+).

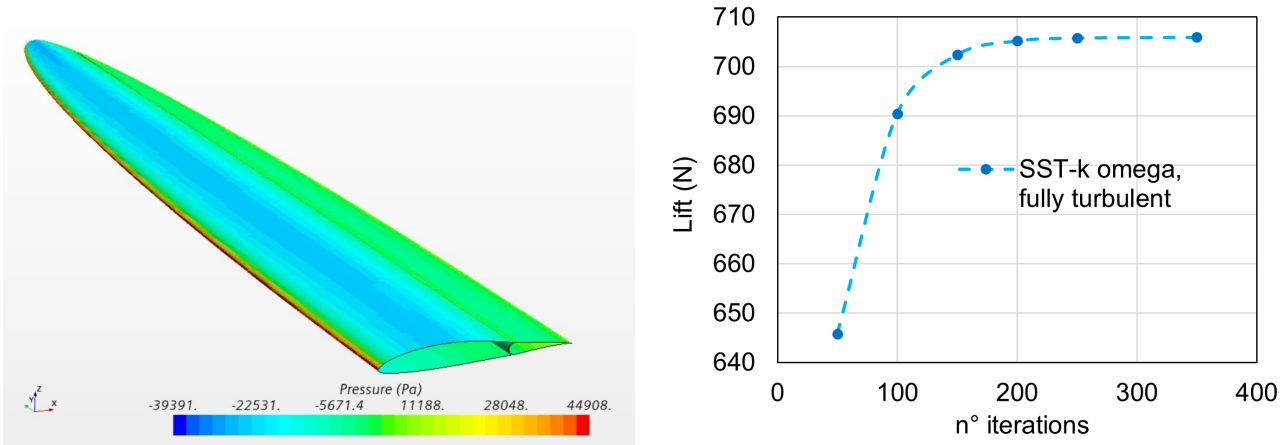

(a) *Pressure distribution on the surface.* **(b)** *Convergence study.*

Figure 14. Mainfoil CFD analysis (Star-CCM+).

5.2.2 Optimization Workflow in modeFRONTIER

Mainfoil optimization workflow, pictured in Figures 15 and 16, consists in the subsequent steps:

- Four geometric inputs (b, A, Δ and flap length) are defined and fed into a Grasshopper node. For each design with different input parameters, a new geometry is created in Grasshopper and exported in a format compatible with the CFD solver (.iges).
- Other eight inputs (b, A and max α for both mainfoil and rudderfoil, lift ratio, and max α_{flap}) are instead fed directly into the VPP (Excel) node to compute the correct pitch and flap angles for each of the two studied conditions (take-off speed and 18 kn).
- These parameters are passed on in vector format into an Inner Loop node (Figure 16), which runs the hydrodynamic simulation twice. CFD model described in §5.2.1 is set through a macro – using CAD geometries, angles α and α_{flap} – the simulation is run and then the solver delivers lift, drag, and cavitation index values.
- The chosen algorithm (*Pilopt*, a proprietary algorithm which encloses multiple numerical investigation strategies) evaluates the outputs at iteration *n* and set the input values for iteration *n+1*.

The optimization strategy consists in maximizing foil efficiency both at take-off and at a reference downwind speed of 18 knots. Lift was set as a constraint to ensure enough lift to sustain the design weight of 130 kg (with a 5% tolerance). Lift ratio value of 78% was used to compute required load on the mainfoil (see Table 3). A total of 65 different designs were created and tested.

Rudderfoil optimization follows the same logic, with a few changes on the input variables: in place of the two variables describing the flap, anhedral depth d was added (this shape parameter is defined in §4.2). 50 designs were run and analyzed, using the same CFD template.

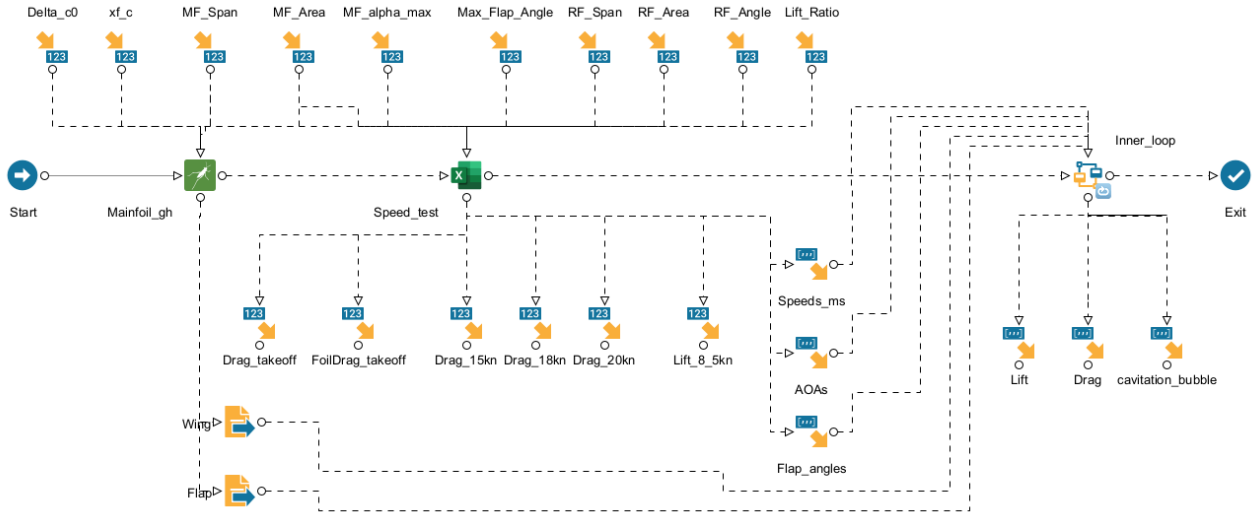

Figure 15. Mainfoil optimization workflow (modeFRONTIER).

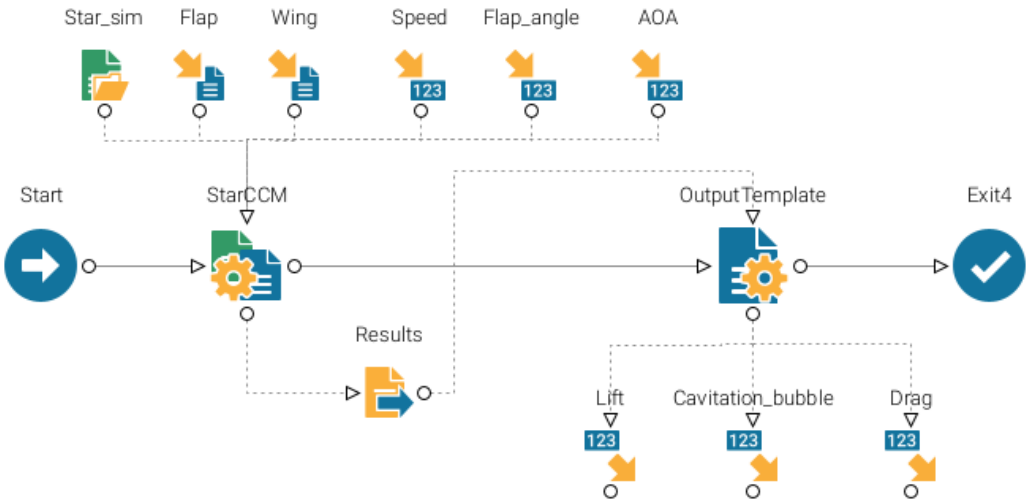

Figure 16. Inner Loop with StarCCM+ (modeFRONTIER).

6 RESULTS

6.1 Evaluation of Best Designs

In the following graph (Figure 17) the data set is shown for the mainfoil optimization process, highlighting the baseline (#0, in blue), design #82 (in red), and design #41 (in light blue), which is regarded as the optimum trade off. Due to the limited amount of wings tested, data distribution doesn't show a well-defined Pareto front. As a result, the final choice was made by picking manually a few of the *Pareto efficient* solutions and comparing them using an higher accuracy CFD model.

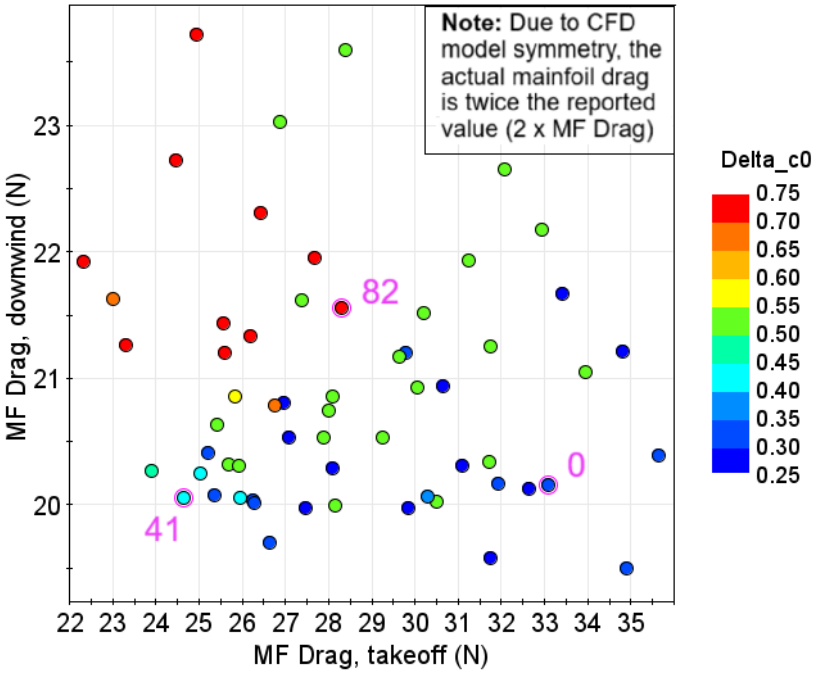

Figure 17. Baseline vs best design mainfoil comparison (modeFRONTIER).

The resulting optimized wings are defined by the geometric features and operating angles shown in Tables 4 and 5. The variation of α for the mainfoil is related to the expected trim by stern happening at take-off, while the design target in foiling mode is set to 1°. On the other hand, rudderfoil angle of attack is a variable which can be adjusted during navigation, as explained in §3.1. This control is achieved by acting on the rudder rake via the tiller extension screw mechanism, typical for Moths.

Table 4. Main geometric parameters, final results.

	b	A	Δ	Flap length	d
Mainfoil	1150 mm	960 cm^2	43%	30%	-
Rudderfoil	800 mm	400 cm^2	30%	-	40 mm

Table 5. Design angles up to 25 knots, final results.

	α	α_{flap}
Mainfoil	3° to 1°	9° to -7°
Rudderfoil	4° to -4°	-

6.2 Final Geometry

The optimization process led to define the shape of the two lifting surfaces. The following task was to design and integrate the bulbs, which function as attachment point for the struts. Given the structural constraints on bulb thickness, in order to reduce the junction drag a smooth surface was modeled. There are essentially two ways to do that, an axisymmetric shape or an airfoil shape (*blended bulb*).

This second option was chosen, keeping roughly the same section as the wing body (the Eppler 393), with only minor modifications. The bulb main dimensions and position relative to the wing were studied using XFLR5 and Star-CCM+, drawing a comparison with the most common Moth configurations. Structural issues were also taken into account. Once the shape was tested and validated, the final hydrofoil was modeled in Rhinoceros, blending the bulb with the lifting surface (Figure 18).

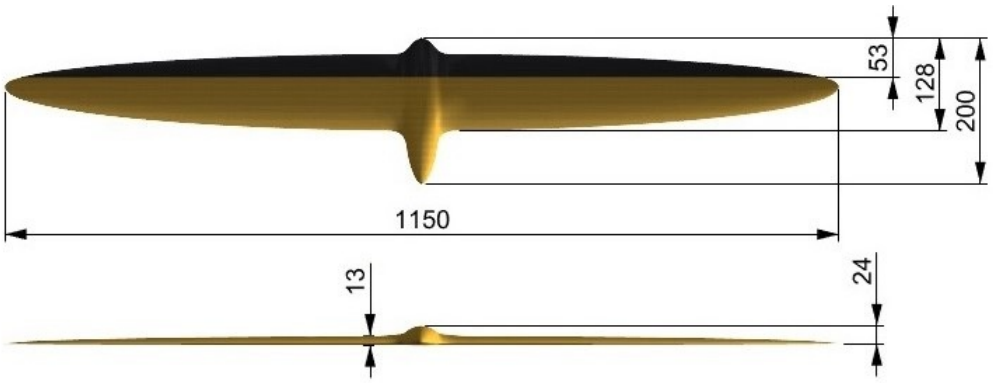

(a) *Mainfoil, top and front view.*

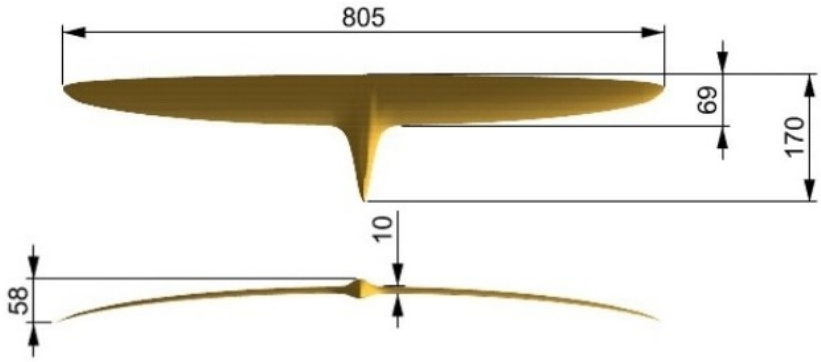

(b) *Rudderfoil, top and front view.*

Figure 18. Optimized design of AST Moth hydrofoils (Rhinoceros).

Drag curve for this final hydrofoil configuration is shown in Figure 19: total resistance data (hull + wings) and sail thrust estimations are computed using the VPP tool described in §3.2. According to this graph, take-off is expected to happen from a minimum true wind speed (TWS) of 6 knots. A more detailed comparison with benchmark foils from Beaver and Zseleczky (2009), base) (Reynolds Averaged Navier Stokes) analyses, is summarized in Figure 20, showing the higher efficiency of AST optimized mainfoil across the entire speed range. Table 6 displays geometric differences between the two sets of foils.

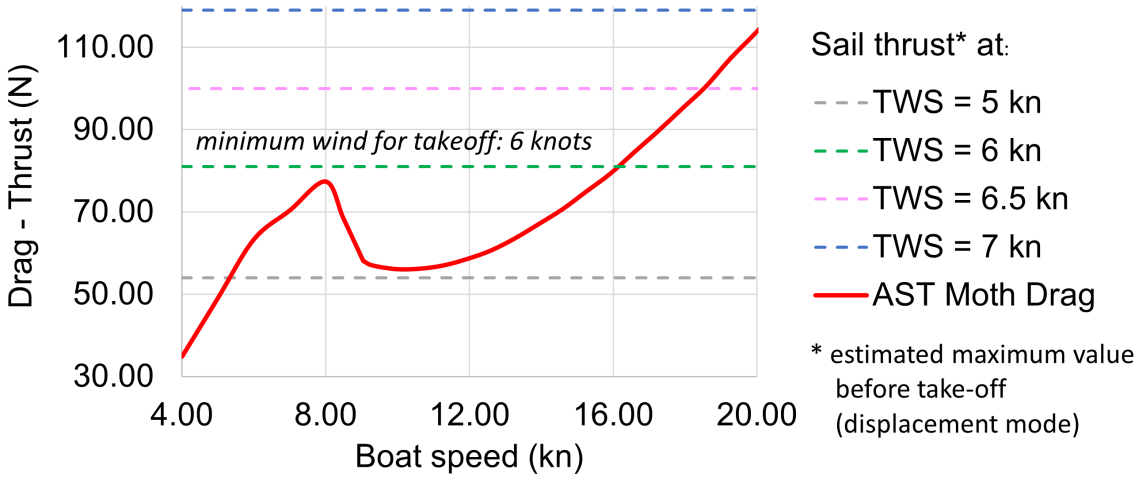

Figure 19. Drag curve and minimum wind intensity for take-off (data from in-house VPP).

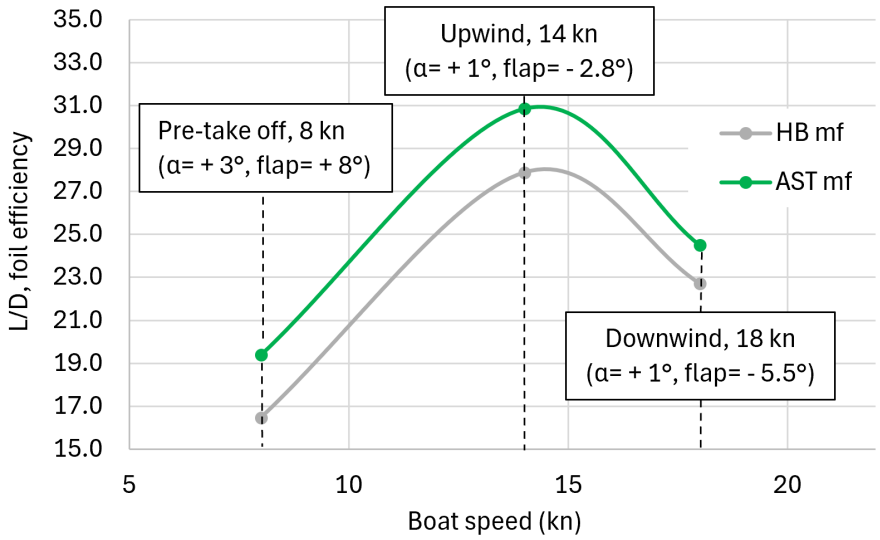

Figure 20. Mainfoil comparison, AST vs Hungry Beaver (data from Star- CCM+).

6.3 Additional Design Aspects

6.3.1 Rudder and Centreboard Design

Also the vertical struts, namely the rudder and centreboard, were included in the design process. Compatibility with a set of foils already available had to be provided. Starting from this assumption, some considerations were made on planform shape: chord was increased in the root area, to improve maneuverability in displacement mode, and reduced in the tip area, to minimize parasitic drag. Planforms were carefully drawn in Rhinoceros so as not to have any excess wetted surface area, with faired curves: the leading edge follows an elliptical course, while the trailing edge is a weighted curve which respects minimum thickness requirements on wing sections. Centreboard and rudder sections has been analyzed in the same way as described in §3.1, leading to: NACA 0012 (root) and NACA 63015 (tip) for rudder; NACA 63012 (root) and NACA 66014 (tip) for centreboard.

Table 6. Dimensional comparison between AST and Hungry Beaver foils.

Mainfoil	Hungry Beaver	AST Moth	difference, %
b (mm)	985	1150	+17%
c_{root} (without bulb, mm)	120	107	-11%
A (cm^2)	1030	960	-7%
λ (-)	9.4	13.8	+47%
Rudderfoil	Hungry Beaver	AST Moth	
b (mm)	880	800	-10%
c_{root} (without bulb, mm)	115	54	-53%
A (cm^2)	806	400	-50%
λ (-)	9.6	16	+68%

6.3.2 Balancing Foils Position

The relative placement of rudderfoil and mainfoil, with respect to the sail plan, is key for flight stability and thus ease of handling during foiling. Vertical position of the foil is directly related to strut length. Longer struts provide more clearance above the water, resulting in easier control and an increase

in the righting arm; however, they entail more load on the strut themselves. Centreboard extends 115 cm from the hull bottom, while the rudder is 110 cm long, from the bottom attachment point. Another vertical parameter is the clearance between rudderfoil and mainfoil, important to ensure that the rudderfoil is closer to the water surface, and thus free from the harmful influence of the mainfoil downwash: this clearance was set to 10 cm (measured with the hull at zero trim).

Longitudinal position of the mainfoil is critical in terms of dynamic stability while foiling and impacts also on the positioning of the mast. After performing a comparative study on a benchmark of existing designs, the mainfoil was placed 144 cm aft of the bow, 44 cm aft of the mast. Finally, forward rake of the struts prevents ventilation (air suction) on the back of the foil: for the centreboard, the design rake was set to a typical value of 7°; conversely, the rudder rake can be adjusted during navigation and it is related to rudderfoil angle of attack, as already discussed. Final configuration is visible in Fig.21.

Figure 21. Render of AST Moth, showing tandem T-foil configuration (Rhinoceros).

6.3.3 Structural Design and Production

The proposed layup for the first couple of foils is a single skin construction, composed as follows: an inner filling of flax fiber composite; a structural shell made with high modulus carbon fiber, alternating unidirectional (along the span) and biaxial plies, the latter especially near the bulb region; a final ply of flax fiber 2x2 twill, covering the whole surface except for the trailing edge, which has to be made with carbon fiber to allow for better sanding.

Figure 22 gives a graphic representation of the mainfoil structure, featuring also a small kevlar strip (yellow) which serves as the flap hinge. This layup had to comply with the requirements stated in §2.2 and §2.3, and it was validated using Finite Element Method (FEM) analysis. Then, a digital model was created, as a tool for the manufacturing phase. Each ply was drawn in Rhinoceros with proper care, taking into account expected thickness values resulting from previous lamination tests.

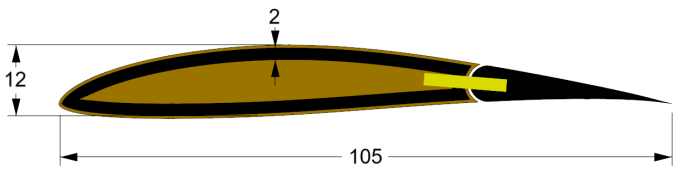

Figure 22. Mainfoil layup: flax, carbon and kevlar (Rhinoceros).

At this point, the manufacturing phase could finally start. Paper templates are printed and used to cut the plies with the right shape in order to fill the mould with the exact amount of material needed. Fiber is impregnated with bio-based epoxy (no pre-preg was used) and placed into the aluminum moulds

– which has been engineered by the Team, and then CNC machined with the help of a supporting company. Vacuum bagging technique is used to compact fibers and extract air and excess resin; after half an hour, the bag is removed and the two aluminum halves are fastened together for the *compression moulding*. After curing, the foils are extracted and finished. The extraction process is pictured in Fig. 23.

Figure 23. Taking the rudderfoil out of the mould (University of Trieste, 2023).

7 CONCLUSIONS

In this paper a methodology applicable to the design and construction of hydrofoils for sailing boats was presented – a method which, through the use of performing fine-tuned design procedures and a multi-criterial approach, can lead to overcome at least partially the paradigm of the *design spiral*.

This has been the first experience with a full foiling concept for Audace Sailing Team. As a result, some aspects of the design and production processes had to be iterated a couple of times, to correct beginner's mistakes and obtain a satisfying result. The multi-fidelity framework adopted starts with simple and effective tools and slowly adds complexity, while converging toward the final configuration: this was key to develop an excellent product in a short period of time, also incorporating specific constraints and parameters that allowed to accurately manage the additional challenge of flax fiber. The final product is a couple of fully submerged hydrofoils, the first being made using flax fiber composite (50% by weight): despite the inherent limitations of the material, the foils proved to have acceptable stiffness and strength. A photo of the first couple of the Audace foils is depicted in Fig. 24.

The hydrodynamic performance, which is the main focus of this study, proved to be satisfying, with reference to both design benchmarks and fellow competitors in the SMC. During tests and races, our prototype (*Bai-Flying Lina*) was sailed by dinghy sailors with almost no previous experience on the foils. However, after a couple of days for quick boat tuning, the boat proved to be very stable on the foils. Take-off speed (around 8.5 knots) was reached even in a 6-7 knots breeze, in accordance with design predictions (Fig. 19), and a top speed of over 20 knots was hit. The boat is still a little slower than commercial Moths, but there is a lot of room for improvements. In the end, *Bai-Flying Lina* and its hydrofoils met all the design goals stated in §2.4: as a consequence, the boat was recognized as the best design of the SuMoth Challenge 2023 by a jury of foiling experts and won the overall first prize, standing out in all three stages: Design, Manufacturing and Racing. Manufacturing phase confirmed that the choice of using flax fiber to replace fiberglass, also in high-performing crafts, is already a feasible alternative. However, the production process presents some threats and has to be approached carefully, especially in order to get the proper thickness of the laminate out of the mould: even a small excess of fabric leads to thicker foils which do not comply with the CAD design.

Figure 24. First couple of Audace flax fiber foils (METSTRADE 2023).

The proposed design approach, coupled with strategic design goals has proven to be not only successful in terms of performance but also versatile over time. In fact, this workflow has been used to further improve the hydrofoils design in 2024 campaign, adapting it to obtain a set of foils optimized for higher speeds and more experienced sailors. Development is currently undergoing to improve the 1.0 version of this design process. For instance, the parametrization has been extended also to wing sections, optimizing a custom hydrofoil section to upgrade efficiency in the desired speed range. This module can be run as stand alone or integrated in the described routine, with a full 2D to 3D coupling: one limitation of the current workflow is, in fact, that the choice of a suitable 2D section is based on assumptions and does not directly take into account what is learned downstream regarding effective operating conditions and 3D design. Another area of improvement is the Static VPP module, which is being translated into code to make it more versatile and compatible with different source input data (es. from CFD solver). In addition to that, a Dynamic Velocity Prediction Program (DVPP) could also be developed to study real non-stationary foiling conditions, inspired by the model proposed by Eggert (2018). Finally, Response Surface Models (RSM, i.e. surrogates) could also be applied to speed up high fidelity stage.

In conclusion, the project described represents an example of what can be a valuable learning opportunity for engineers and designers *in the making*, offering both the freedom to explore innovative ideas and the motivation and resources to turn them into real products. Hopefully, the work presented in these pages will be useful as a reference point for future challenges involving student teams, and also in the broader context of sports and engineering competitions.

ACKNOWLEDGEMENTS

The project described in this pages was only possible thanks to the support of the University of Trieste, Engineering and Architecture Department professors and our thesis supervisors. Our gratitude goes to them and to all AST sponsors, for believing in our team's work. Finally, the warmest thanks are for our fellow AST students and alumni, who have been working hard since 2019 to create such a unique reality. Figure 25 shows the 2023 Audace Sailing Team at the launch of our first Moth, *Bai-Flying Lina*.

Figure 25. Audace Sailing Team (Yacht Club Adriaco, 2023).

REFERENCES

11th Hour, I. T. (2022). *Sustainable Design and Build Report*. URL: https://11thhourracing.org/app/uploads/2022/12/211202-11th-hour-racing-team-IMOCA-Sustainable-Design-and-Build-Presentation-.pdf (visited on 11/17/2024).

AST (2025). *Audace Sailing Team*. URL: https://audace.units.it/ (visited on 05/18/2025).

Bagué, A., Degroote, J., Demeester, T., and Lataire, E. (2021). Dynamic Stability Analysis of a Hydrofoiling Sailing Boat using CFD. en. *Journal of Sailing Technology* 6.01. DOI: 10.5957/jst/2021.6.1.58.

Baley, C. et al. (2019). Specific features of flax fibres used to manufacture composite materials. *International Journal of Material Forming*. DOI: https://doi.org/10.1007/s12289-018-1455-y.

Baley, C., Gomina, M., Breard, J., Bourmaud, A., and Davies, P. (2020). Variability of Mechanical Properties of Flax Fibres for Composite Reinforcement. A Review. *Industrial Crops and Products*. DOI: 10.1016/j.indcrop.2019.111984. URL: https://doi.org/10.1016/j.indcrop.2019.111984.

Beaver, B. and Zseleczky, J. (2009). Full scale measurements on an hydrofoil International Moth. *19th Chesapeake Sailing Yacht Symposium*. DOI: 10.5957/CSYS-2009-013.

Binns, J. R. et al. (2008). The effect of heel angle and free surface proximity on the performance and strut wake of a moth sailing dinghy rudder T-foil. en. *3rd High Performance Yacht Design Conference*.

Blier, T., Troalen, W., Baley, C., and Baral, N. (2025). Flax Fiber Reinforced Composites in Boat Building: A Comprehensive Review and Application-Oriented Testing. *25th Chesapeake Sailing Yacht Symposium*. SNAME. DOI: 10.5957/CSYS-2025-017.

Bonetti, M. (2024). Design, hydrodynamic optimization and manufacturing of a flax fiber International Moth. en. University of Trieste. URL: https://www.academia.edu/122622611/Design_hydrodynamic_optimization_and_manufacturing_of_a_flax_fiber_International_Moth.

Cantamessa, M. (2024). The Rhinoceros and the Grasshopper: hull shape parametrization for geometric optimization of a Moth. Bachelor's degree in Naval Architecture and Maritime Engineering. University of Trieste.

Castegnaro, S. and Basile, M. (2017). A bio-composite racing sailboat: materials selection, design, manufacturing and sailing. en. DOI: https://doi.org/10.1016/j.oceaneng.2017.01.017.

Davies, P. et al. (2022). Seawater aging of infused flax fibre reinforced acrylic composites. *Composites Part C: Open Access*. DOI: 10.1016/j.jcomc.2022.100246.

Day, S., Cocard, M., and Troll, M. (2019). Experimental measurement and simplified prediction of T-foil performance for monohull dinghies. en. *23rd Chesapeake Sailing Yacht Symposium*.

De Carli, B. (2024). Hydrofoil CFD simulation framework, developed to be implemented into an optimization cycle. it. Bachelor's degree in Naval Architecture and Maritime Engineering. University of Trieste.

Drela, M. (1989). XFOIL: an Analysis and Design System for Low Reynolds Number Airfoils. *Low Reynolds Number Aerodynamics*. Lecture Notes in Engineering 54. Springer-Verlag. URL: https://web.mit.edu/drela/Public/papers/xfoil_sv.pdf/.

Drela, M. and Youngren, H. (2001). *XFOIL 6.9 User Guide*. URL: https://web.mit.edu/drela/Public/web/xfoil/.

Eggert, F. (2018). Flight Dynamics and Stability of a Hydrofoiling International Moth with a Dynamic Velocity Prediction Program (DVPP). DOI: 10.13140/RG.2.2.20154.03524.

Ferletti, S. (2023). Hydrofoil optimization for a racing sailboat. it. Master's degree in Naval Architecture and Maritime Engineering. University of Trieste.

Findlay, M. W. and Turnock, S. R. (2008). Development and use of a Velocity Prediction Program to compare the effects of changes to foil arrangement on a hydro-foiling Moth dinghy. en. *Innovation in High Performance Sailing Yachts*. URL: https://eprints.soton.ac.uk/52462/1/Findlay_Turnock_Foil_VPP.pdf.

Giovannetti, L. M. (2017). Fluid structure interaction testing, modelling and development of Passive Adaptive Composite foils. en. PhD thesis. University of Southampton. URL: https://eprints.soton.ac.uk/412651/1/Thesis_with_minor_corrections_v2_compressed.pdf.

Gon, R. (2021). Morphing foil optimization for an International Moth: hydrodynamic study. it. Master's degree in Naval Architecture and Maritime Engineering. University of Trieste.

Greenboats (2025). *Greenboats*. URL: https://www.green-boats.de/ (visited on 05/18/2025).

Guedes Soares, C. and Santos, T. (2022). Structural analysis of a 'Foiling Moth' sailing dinghy hydrofoil. en. *Trends in Maritime Technology and Engineering*. ISBN: 978-1-00-332027-2. URL: https://www.taylorfrancis.com/books/9781003320272/chapters/10.1201/9781003320272-21.

IMCA (2017). *International Moth Class Rules*. URL: http://www.moth-sailing.org/history/rules-and-documents/ (visited on 05/09/2024).

Inguglia, S. (2021). CFD analysis of a racing sailboat. Master's Degree. Polytechnic of Turin. URL: https://webthesis.biblio.polito.it/secure/20008/1/tesi.pdf.

Larsson, L., Eliasson, R. E., and Orych, M. (2022). *Principles of yacht design*. Londra: Adlard Coles Nautical.

Menter, F. R. (1994). Two-Equation Eddy-Viscosity Turbulence Models for Engineering Applications. *AIAA Journal*.

Mozzy Sails (2022). *ETNZ's New Wing: the Banana foil!* URL: https://www.youtube.com/watch?v=zL0iEpL5n1w (visited on 11/19/2024).

Muzio, V. (2021). Morphing foil optimization for an International Moth: structural study. it. Master's degree in Naval Architecture and Maritime Engineering. University of Trieste.

Neri, D. (2024). *How to sail a Moth*. en. URL: https://www.northsails.com/it-it/blogs/north-sails-blog/how-to-build-your-moth-skills-north-sails (visited on 06/18/2024).

NLcomp (n.d.). *Northern Light Composites*. it-IT. URL: https://northernlightcomposites.com/.

Nobile, U. (1954). *Elementi di aerodinamica - Principles of Aerodynamics*. Ed. by u. s. Stato maggiore dell'Aeronautica. Vol. 1. Roma: Libreria dello Stato.

ORC (2016). *ORC VPP Documentation*. Offshore Racing Congress. URL: www.orc.org/rules/ORC%5C%20VPP%5C%20Documentation%5C%202016.pdf.

Parmegiani Della Corte, A. (2023). Preliminary design of a racing hydrofoil. it. Bachelor's degree in Naval Architecture and Maritime Engineering. University of Trieste.

Pourcheron, L. (2010). The first flax-fiber reinforced composite racing boat : when performance meets sustainability. en. *Huntsman advanced materials Report*. URL: https://www.octima.it/wp-content/uploads/2016/01/10EES_Hunstman.pdf.

Prabahar, N. S. S., Persson, A., and Larsson, L. (2022). Split-Flaps – a Way to Improve the Heel Stability of T-Foil Supported Craft. en. *Journal of Sailing Technology* 7.01. ISSN: 2475-370X. DOI: 10.5957/jst/2022.7.1.1.

Souppez, J.-B. R. G., Ruiz, P. R., Raihan, M. A., and Oh, D. (2025). Towards the Regulatory Inclusion of Sustainable Composite Material Available. *25th Chesapeake Sailing Yacht Symposium*. Annapolis, Maryland, USA. DOI: 10.5957/CSYS-2025-018. URL: https://doi.org/10.5957/CSYS-2025-018.

Speer, T. (2001). *Generic Hydrofoil Trade Study*. URL: http://www.tspeer.com/Hydrofoils/generic.pdf.

SuMoth Association (2022). *SuMoth MasterClass #01 - KISS of the SuMoth with Julien Chaussée*. URL: https://www.youtube.com/watch?v=RJvRpjtmn9Y.

SuMoth Association (2024). *SuMoth Challenge Rules, v24 r1.1*. URL: https://sumoth.org/rules/.

Tannenberg, R., Turnock, S. R., Hochkirch, K., and Boyd, S. W. (2023). VPP Driven Parametric Design of AC75 Hydrofoils. *Journal of Sailing Technology*, pp. 161–182. DOI: 10.5957/jst/2023.8.9.161.

Trincas, G. (2022). Keynotes on Ship Design, lessons at the University of Trieste.

Website, I. (2024). *Impact reduction rule*. en. URL: https://www.imoca.org/en/news/news/imoca-becomes-the-first-class-in-sailing-to-impose-an-impact-reduction-rule-on-boat-construction.

Yiu, K. and Giles, M. (1995). Simultaneous Viscous-Inviscid Coupling via Transpiration. *Journal of Computational Physics* 120.2, pp. 157–170. ISSN: 0021-9991. DOI: https://doi.org/10.1006/jcph.1995.1156.